Hydrothermal phosphate vein-type ores from the southern Central Iberian Zone, Spain: Evidence for their relationship to granites and Neoproterozoic metasedimentary rocks.

Elena Vindel [a,*], Eva Chicharro [a], Carlos Villaseca [b], José Ángel López-García [a], Virginia Sánchez [c]

[a] Dpt. Cristalografía y Mineralogía, Facultad Ciencias Geologicas, Universidad Complutense, 28040 Madrid, Spain
[b] Dpt. Petrología y Geoquímica, Facultad Ciencias Geologicas, Instituto de Geociencias (UCM, CSIC), Universidad Complutense, 28040 Madrid, Spain
[c] Centro Tecnológico de Repsol, Móstoles, Madrid, Spain

A b s t r a c t

Hydrothermal quartz–apatite veins, called "Iberian-type", occur exclusively in the southern Central Iberian Zone. This study presents a multidisciplinary approach leading to the mineralogical, fluid inclusions, and geochemical characterization of these veins from two representative areas, Logrosán and Belvís–Navalmoral, in order to estab-lish their relationship with nearby phosphorous-rich granites and apatite in Neoproterozoic metasediments. The mineral assemblage of these veins comprises quartz, apatite, minor sulfides, dolomite, Fe–Mg-carbonates and Fe–Mn-oxides. Three texturally different types of apatite have been recognized in the veins: apatite I showing prismatic habit associated with minor sulfides, apatite II occurring as white fibrous radial crystal aggregates called "dahllite", and apatite III as grayish to greenish hexagonal crystals. Hydrothermal apatite from veins (H-apatite) is enriched in Sr and depleted in Mn–Y–REE–Th–U–Pb compared to magmatic apatite (M-apatite) from the granitic plutons. However, trace element compositions of apatite from metasedimentary phosphorous-rich levels or nodules (S-apatite) of the Schist–Greywacke Complex show similar characteristics to the H-apatite, although the H-apatite stands out for its relatively high Sr-contents. This relative Sr enrichment in H-apatite is interpreted as inherited from both phosphate in Neoproterozoic metasediments (S-apatite) and carbonate levels. REE, fluid inclusion and stable isotope data are consistent with a long episode of hydrothermal activity implying cooling and dilution processes while interacting with phosphate-rich shale and carbonate beds in the SGC. Fluid inclusion study undertaken on hydrothermal apatite and quartz reveals the presence of aqueous low salinity fluids (0.2–6.7 wt.% NaCl equiv.) at moderate to low Th (125–350 °C). All available data point at a recycling event of the southern CIZ metasediments (the SGC) during post-Variscan hydrothermal fluid circulation as the more plausible origin of the phosphate vein-type mineralizations.

Keywords: Phosphate; Hydrothermal; Neoproterozoic metasediments; Apatite chemistry

1. Introduction

Western-central Spain was one of the most important phosphate producer regions in Europe from the 1850s to the end of the Second World War, involving more than 50% of the Spanish production (Boixereu, 2004). At this moment the sedimentary phosphate deposits of Bucraa in Western Sahara were discovered, becoming the mean source of supply for phosphate industry. Since the discovery of the Bucraa phosphate deposits, the mines of western Spain have remained inactive, except for small operations. Two types of mineralization were exploited: (1) quartz–apatite veins of hydrothermal origin and (2) stratabound deposits related to Lower Carboniferous carbonate rocks filling karstic cavities. This study focuses on the hydrothermal veins about which there are only old and incomplete studies in the liter-ature (Aizpurúa et al., 1982; Rambaud et al., 1983). Among the main mining districts of this type, the most productive during the first part of the 20th century was Logrosán located in the south of the studied area (Fig. 1) (Boixereu, 2003). Other small occurrences, such as Belvís de Monroy, Millanes and Navalmoral de la Mata, are situated in the north of the studied district (Fig. 1).

Hydrothermal phosphate veins occur exclusively in the southern Central Iberian Zone (CIZ), which is the innermost part of the Iberian Variscan Massif. These ore deposits are spatially related to peraluminous and perphosphorous granitic intrusions as intra or extra-batholitic veins. The phosphate veins, so-called "Iberian-type" by Aizpurúa et al. (1982),

* Corresponding author. Tel.: +34 913944871; fax: +34 913944872.
E-mail addresses: evindel@ucm.es (E. Vindel), echicharro@ucm.es (E. Chicharro), granito@ucm.es (C. Villaseca), jangel@ucm.es (J.Á. López-García), virgina.sanchez@repsol.com (V. Sánchez).

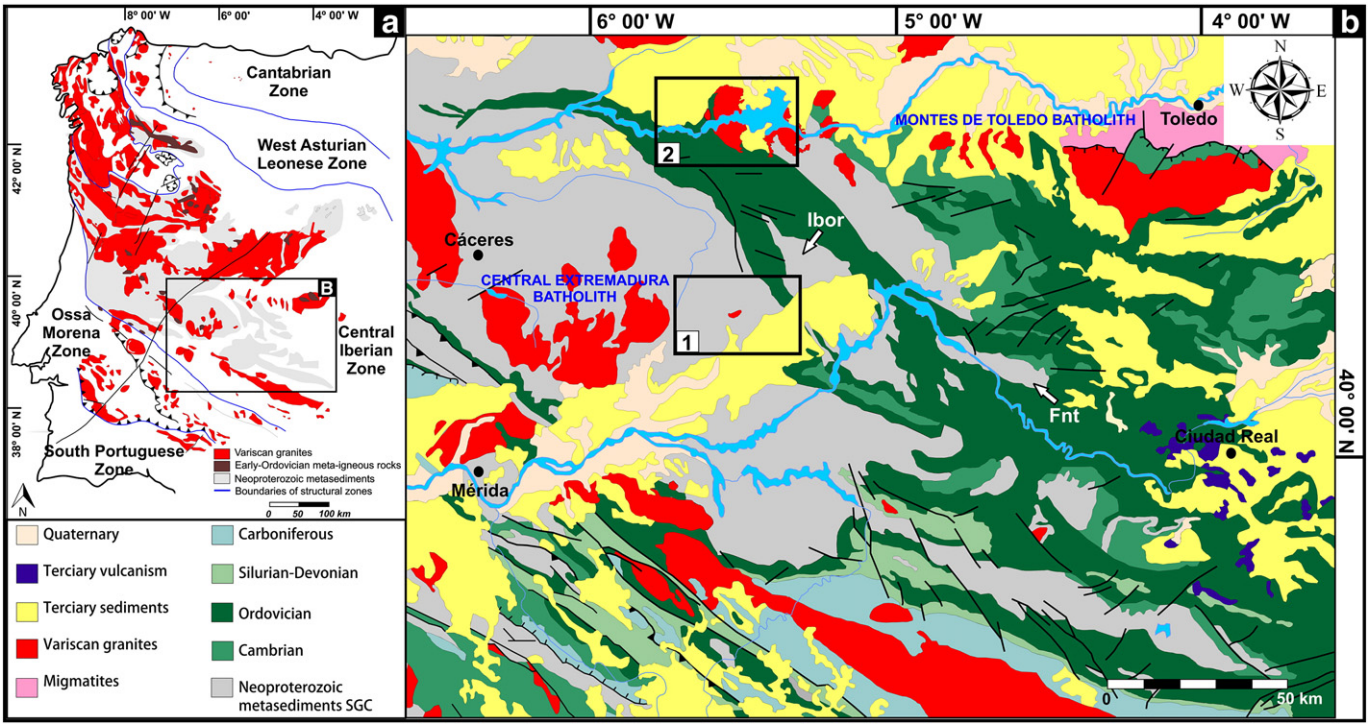

Fig. 1. (a) Location of the Central Iberian Zone (CIZ) in the Iberian Massif. (b) Regional geological sketch displaying the two studied areas: (1) Logrosán and (2) Belvís–Navalmoral. Outcrops cited in text are Ibor: carbonate unit; Fnt: Fontanarejo phosphate levels in Neoproterozoic sediments.
Modified from Rodriguez et al. (2008).

are of relevant importance since they have been recognized only in this part of the Variscan belt of Western Europe. These veins are of hydrothermal origin and their relationship with the associated granites remains unclear.

The present contribution (1) describes the main features of quartz–apatite vein deposits, (2) analyzes the apatite chemistry with REE data that are specially useful to gather information about the source of these elements, (3) compares the apatite chemistry from the veins (hydrothermal, H-apatite) with the apatite chemistry from related granites (magmatic, M-apatite) and from apatite in the Neoproterozoic metasediments (S-apatite), (4) analyzes the compositional variation of arsenopyrite in order to be used as a geothermometer, (5) characterizes the hydrothermal system through fluid inclusion analyses, and (6) deduces information on possible sources of the mineralizing fluids and protoliths involved through stable isotope analysis. Ultimately, the obtained results allow us to place the phosphate ores within the hydrothermal activity of the CIZ and to establish their relationship with phosphorous-rich granites and the Neoproterozoic metasediments.

For this purpose, this study has been focused on two representative areas, Logrosán in the South, and Belvís de Monroy (Belvís)–Navalmoral de la Mata (Navalmoral) in the North of the Cáceres province (Fig. 1). In addition, the phosphorite occurrences of sedimentary origin in the upper part of the regional Schist–Greywacke Complex (SGC) have also been analyzed for comparative purposes.

2. Geological setting

The Iberian Massif is the southwestern extension of the European Variscan Belt and one of the largest domains of the Variscan orogen. Large volumes of granitoids were emplaced during post-collisional stages of the Variscan Orogeny, mostly syn- or clearly late to the D_3 event (e.g., Dias et al., 1998). The Logrosán, Belvís and Navalmoral plu-tons are situated in the southern part of the CIZ (Julivert et al., 1974), in the Iberian Massif (Fig. 1). They are biotite-bearing monzogranites to two-mica peraluminous leucogranites (S-type granites) with a marked perphosphorous trend.

The Logrosán granite is one of the post-kinematic bodies of the Central Extremadura Batholith, which belongs to the epizonal domains of the CIZ (Castro, 1985). It is a small body, of no more than 4 km^2 in outcrop, which is a typical felsic cupola affected by an intense hydrothermal alteration represented by the tourmalinization, greisenization and formation of an intragranitic stockwork of Sn–(Ta)–W veins (Chicharro et al., 2013). Apatite is an accessory mineral in those granites, mostly included in plagioclase and K-feldspar. The Logrosán granite intrudes the Neoproterozoic metasedimentary sequence of the SGC which is characterized in this area by a monotonous decimetre- to centimetre-scale alternation of greywackes and slates with minor presence of sandstones and conglomerates. A Variscan low-grade regional metamorphism (Chl-Bt) has affected the Neoproterozoic country rocks while the emplacement of the granitic body has produced a contact metamorphism characterized by an inner hornfels zone and an outer zone of spotted phyllites and chlorite schists.

The Belvís and Navalmoral granites are located on the western segment of the Montes de Toledo Batholith (MTB) intruding into low-grade Neoproterozoic and Lower Paleozoic metasedimentary rocks and causing remarkable contact aureoles (Villaseca et al., 2008). The contact metamorphism induced by the Belvís intrusion suggests an epizonal level of granite emplacement with pressures of crystallization below 2 kbar (Merino et al., 2013). The later Navalmoral granite cross-cuts the aplopegmatitic dyke-system associated with the Belvís pluton indicating a similar shallow level of emplacement. The Belvís massif is composed of two-mica highly fractionated leucogranites, markedly P-rich (P_2O_5: 0.63–0.85 wt.%), and involves complex accessory mineralogy (Merino et al., 2013). The Navalmoral pluton is mainly composed of biotite granite with variable amounts of K-feldspar megacrysts and lower P_2O_5 content (0.29–0.38 wt.%) than the Belvís granite (Villaseca et al., 2008). The intrusion age of the Belvís granite has been established at ca. 314 Ma, in agreement with the post-tectonic Variscan character of most granite intrusions of central Spain (Orejana et al., 2011). Recently

the Navalmoral and Logrosán granites have been dated by U–Pb geochronology on zircon separates yielding ages of 307 and 308 Ma, re-spectively (Chicharro et al., 2013, accepted for publication; Merino et al., accepted for publication).

The Neoproterozoic metasedimentary rocks of the Schist–Greywacke Complex (SGC), into which the Variscan granites intruded, make up a thick (up to 11 km) sandstone–shalesequencewithsomeconglomerate and carbonate intercalations (e.g., Rodríguez-Alonso et al., 2004). The SGC metapelites are characterized by a slightly higher P content than other metasedimentary series of the northern CIZ (Villaseca et al., 2014), and phosphorite deposits are restricted to this sequence. Among them, the Fontanarejo (Fnt) and Horcajo de los Montes phosphate deposits that appear interbedded in Neoproterozoic metasediments of the SGC can be highlighted (Fig. 1). They are constituted by phosphate levels that show organosedimentary structures (oncolitic-type) as interlayers in greywackes, shales, conglomerates, quartzites and limestones of the SGC. The morphology and the petrology of these deposits support their interpretation as tidal channel fillings (Gabaldón López et al., 1986; Perconig et al., 1983, 1986).

3. Characteristics and mineralogy of the veins

The Logrosán, Belvís and Navalmoral hydrothermal phosphate veins are located within granites or in the contact aureole between the granites and their host-rocks (Locutura and Alcalde, 2007). The main feature of the three deposits is the presence of quartz and white fibrous radial crystal aggregate apatite, called “dahllite”.

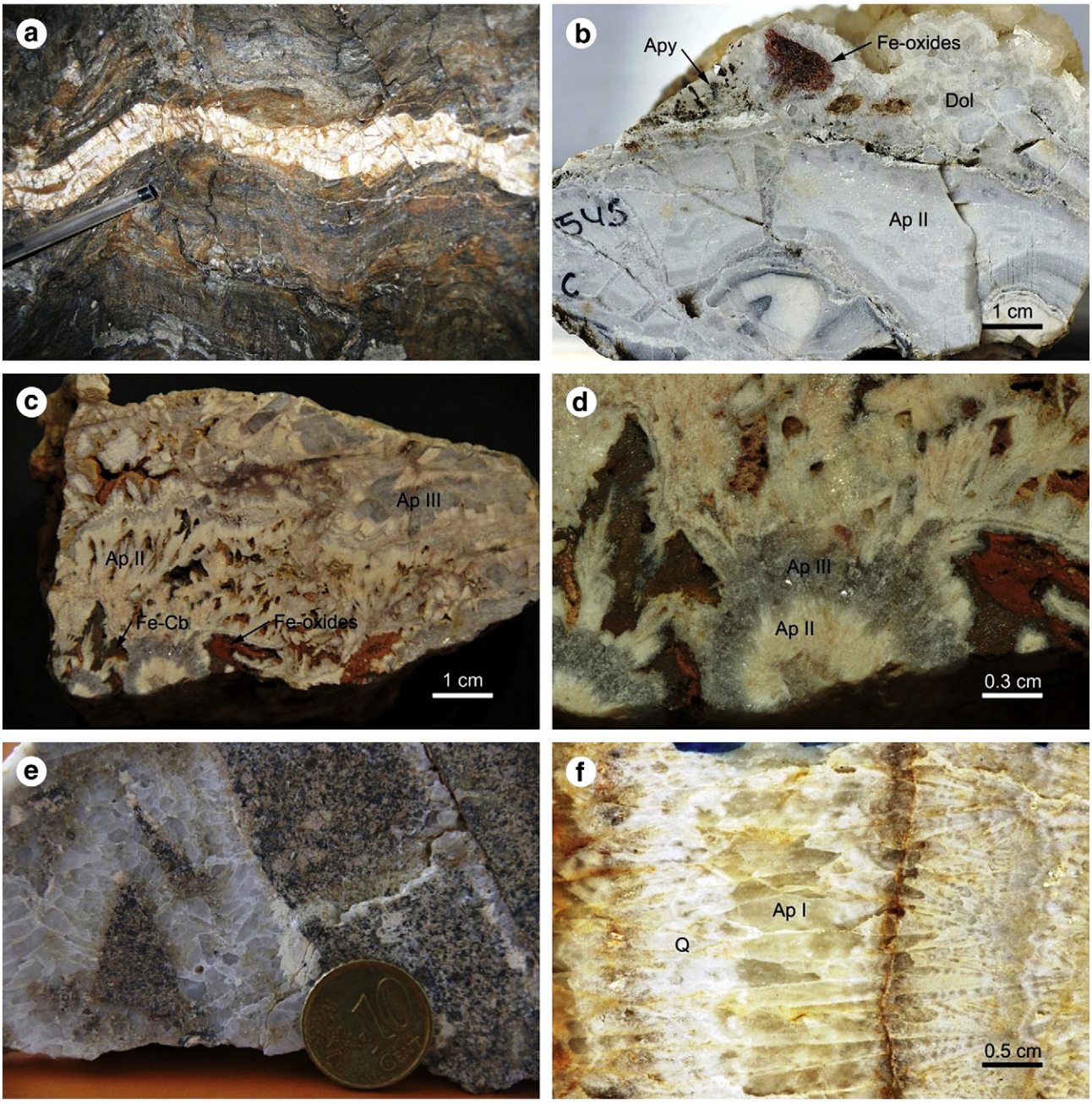

Fig. 2. (a) Sinuous quartz–apatite vein hosted in the SGC. Logrosán. (b) Colloform texture formed by white fibrous apatite, “dahllite” (Ap II). On top dolomite (Dol), arsenopyrite (Apy) and Fe-oxides can be observed. Logrosán. (c) Fibrous apatite (Ap II) intergrown with grayish apatite crystals (Ap III). Fe-oxides and Fe-carbonates (Fe-Cb) can be observed. Belvís. (d) Detail of (c) showing columnar structure formed by grayish apatite crystals (Ap III) surrounding “dahllite” (Ap II). (e) Quartz–apatite veins crosscutting the Navalmoral granite. (f) Prismatic apatite crystal (Ap I) intergrown with drusy quartz (Q). Navalmoral.

The Logrosán deposit (Costanaza mine) is hosted in Neoproterozoic units (SGC) close to the Logrosán granite contact. The ore is structurally controlled and occurs as N20–75°E individual veins and veinlets with vertical to subvertical dip and from few centimeters to 3 m wide. Most veins show sinuous outlines (Fig. 2a), stockworks and brecciated struc-tures. Hydrothermal alteration (silicification and dolomitization) has been observed in the enclosing rocks. The mineralogy of this deposit is the most complex of the studied veins and comprises quartz, apatite, minor sulfides (arsenopyrite, chalcopyrite, pyrite, marcasite), dolomite, calcite, Fe–Mg carbonates, and Fe–Mn-oxides.

The Logrosán veins are characterized by successive bands alternating colloform (Fig. 2b) and crustiform apatite, and fine drusy quartz indica-tive of successive re-opening. There are two texturally different types of apatite: (1) Apatite I, showing prismatic habit, is present as fine white crystals in the edge and the center of the veins; (2) apatite II (dahllite) is the dominant type in the ore (Fig. 2b). Sulfides are minor components restricted to the contact of the enclosing rocks in apparent relation to "saddle" dolomite and minor calcite. Arsenopyrite is scarce, concentrated in the margins of the veins and occurring as small (b5 mm) idiomorphic crystals intergrown with cubes or truncated cubes of pyrite. Other sulfides include chalcopyrite and marcasite, all of which occur along the inner margin of the veins.

Quartz–apatite Belvís veins appear not only within the SGC but also in the Belvís granite (extra and intra-batholitic veins) as few centimeter veinlets along N160–170°E. In addition to Aps I and II, a typical grayish to greenish hexagonal apatite (Ap III) crystals could be recognized (Fig. 2c). Columnar structures formed by Ap III crystals surrounding "dahllite" are common in the Belvís veins (Fig. 2d). Ap III displays some concentration of fluid inclusions suitable for a microthermometric study. Remarkably, little quartz crystals (b1 mm) appear intergrown with apatite. An alteration mineral assemblage of Fe–Mn-oxide and siderite–magnesite is found as replacement of primary minerals or in open space fillings.

Centimetre-scale intrabatholitic quartz–apatite veins following N20–40° E fractures can be observed within the Navalmoral granite (Fig. 2e). Ap I is the predominant type in these veins, alternating with drusy quartz (Fig. 2f) and with dahllite (Ap II). A generalized sequence (Logrosán, Belvís and Navalmoral) of mineralizing events can be in-ferred after the textural relationship between the minerals described above (Fig. 3).

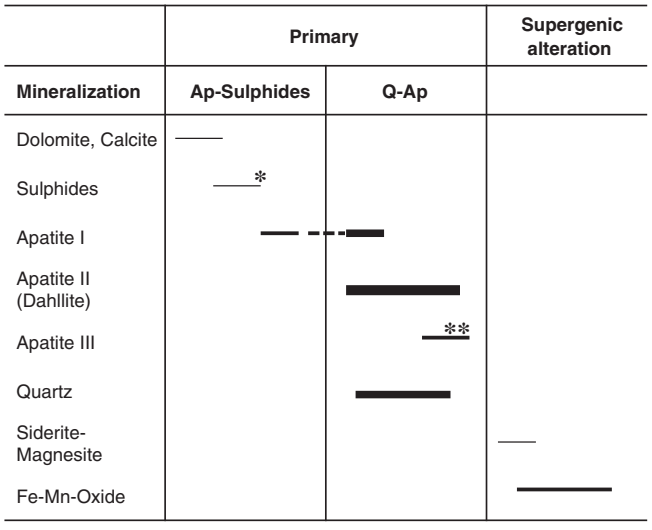

Fig. 3. Generalized paragenetic sequence scheme for the quartz–apatite vein deposits. *Only in Logrosán. **Only in Belvís.

4. Analytical methods

Representative samples of apatite were collected on the Logrosán galleries and on surface mine exposures from Belvís and Navalmoral veins and have been investigated using a variety of analytical techniques. In order to compare the chemistry of hydrothermal (H), magmatic (M) and sedimentary (S) apatites of the area, electron microprobe (EMP) and laser ablation inductively coupled plasma mass spectrometry (LA-ICP-MS) analyses have been performed on these minerals.

Major and minor element contents of apatite, arsenopyrite, pyrite and chalcopyrite were determined using an EMP JEOL Superprobe JXA-8900M, employing wavelength dispersive spectrometry at the Centro Nacional de Microscopía Electrónica, Universidad Complutense de Madrid. Analytical conditions were an accelerating voltage of 15 kV, an electron beam current of 20 nA and a beam diameter of 5 μm. The following minerals were used as standards: sillimanite, albite, almandine, kaersutite, microcline, ilmenite, fluorapatite, scapolite, galena, anglesite, nickeline, AsGa, HR-160 (Co–Ni–Cr), chalcopyrite, Zn, Mo, Ag, Cd, Sb, Bi_2Te_3, cinnabar, and hutchinsonite. Corrections were made using the ZAF method.

Trace element analyses of apatite from the Belvís, Logrosán and Fontanarejo outcrops were conducted by LA-ICP-MS at the Geochronol-ogy and Isotope Geochemistry—SGIker facility of the University of the Basque Country (UPV/EHU Spain) using the method described by Ábalos et al. (2012) and García de Madinabeitia et al. (2013). The anal-yses involved the ablation of minerals in ca. 90 μm thick petrographic sections with a NewWave UP213 Nd:YAG laser ablation system coupled to a Thermo Fisher Scientific XSeries 2 quadrupole ICP-MS instrument with enhanced sensitivity through a dual pumping system. Spot diam-eters of ca. 40 μm associated to repetition rates of 10 Hz and laser fluence at the target of ca. 5 J/cm^2 were used for the analysis. The NIST SRM 614 silicate glass and Durango apatite were used for quality control of the results assuming major and trace element concentrations report-ed by Jochum et al. (2011) and Trotter and Eggins (2006), respectively. Raw data were processed using Glitter 4.4.2 (Jackson et al., 2004; van Achterbergh et al., 2001) and the Ca values obtained by an electron microprobe on the same spots.

The trace element apatite compositions of Navalmoral samples were obtained by LA-ICP-MS at the Natural History Museum of London (NHM, London, UK) using an Agilent 7500CS ICP-MS coupled to a NewWave UP213 laser source (213 nm frequency-quadrupled Nd–YAG laser). The diameter of the laser beam was 30 μm. A 40 s gas blank was analyzed first to establish the background, followed by 50 s measurements for the remainder of the analysis. Each analysis was normalized to Ca using concentrations determined by the electron microprobe. Relative element sensitivities were calibrated by a NIST 612 glass standard. See Jeffries (2001) for a detailed discussion of the LA-ICP-MS analytical technique. All the results of REE concentration were normalized to chondrite values after McDonough and Sun (1995).

Microthermometric studies of fluid inclusions were carried out on doubly polished wafers (300 μm) with a Linkam THMSG 600 heating–freezing stage (Shepherd, 1981). The stage calibration was based on the melting point of solid standards at T N 25 °C and natural and synthetic inclusions at T b 0 °C. The rate of heating was monitored in order to obtain measurement precision of ±0.2 °C during freezing and ±1 °C when heating within the 25–400 °C temperature range. The salinity of H_2O–NaCl inclusions reported as equivalent weight percent NaCl (wt.% NaCl equiv.) was calculated from microthermometric data (ice melting, $T_m$ice) using the equations from Bodnar (1993).

Quartz from Logrosán and Navalmoral veins and 6 whole rock samples were analyzed for $^{18}O/^{16}O$ at the Stable Isotope Laboratories of the Salamanca University (Spain). Quartz has been separated by handpicking after crushing to 80–120 mesh. Unfortunately, the difficulty to separate quartz from apatite in the Belvís samples prevents the $^{18}O/^{16}O$ analyses in these veins. $^{18}O/^{16}O$ determinations were carried out using a laser fluorination procedure, involving total sample reaction with excess ClF_3

(Borthwick and Harmon, 1982) using a CO_2 laser as a heat source (in excess of 1500 °C; following Sharp, 1990). This O_2 was then converted to CO_2 by reaction with hot graphite (Clayton and Mayeda, 1963) and then analyzed on-line by a VG-Isotech SIRA-II mass spectrometer. Reproducibility is better than ±0.3‰ (1σ), based on repeat analyses of internal and international standards during sample runs. CO_2 gas liberated from a saddle dolomite sample from Logrosán was collected after reacting with 103% H_3PO_4 (McCrea, 1950) for the determination of $^{13}C/^{12}C$ and $^{18}O/^{16}O$ isotope compositions. Oxygen and carbonate isotope ratios were measured in a VG-Isotech SIRA-II mass spectrometer. Results are reported in standard notation ($\delta^{18}O$, $\delta^{13}C$) in per mil (‰) deviations from the VSMOW and VPDB standards.

5. Results

5.1. Apatite chemistry

Apatite is a widespread accessory phase in igneous rocks and may incorporate significant amounts of trace elements, Sr, Th, U and rare earth elements (REEs) (e.g., Belousova et al., 2002; Chu et al., 2009; Rønsbo, 2008). Major and trace element compositions of selected H-, M- and S-apatites are summarized in Tables 1 and 2.

All analyzed apatite types are fluorapatite (3–4 wt.% F). High F and lower Cl contents are characteristic of apatite from S-type granites (Sha and Chappell, 1999). Major constituents of apatite, CaO and P_2O_5, show little variation. Values range preferably from 50 to 56 wt.% CaO and 40 to 42 wt.% P_2O_5 in H- and S-apatites, and from 51 to 55 wt.%CaO and 40 to 44 wt.% P_2O_5 in M-apatite. SiO_2, Na_2O and MgO contents are extremely low and mostly below the detection limit in all apatite types. FeO and MnO values in M-apatite (0.2 to 1.4 wt.% FeO and 0.4 to 3 wt.% MnO) are markedly higher than those in H- and S-apatites (b0.02 to 0.2 wt.% FeO and b0.01 to 0.3 wt.% MnO) (Tables 1, 2). H-apatite is rich in strontium (0.3–3.9–4 wt.% SrO) in comparison to M-apatite (0.01–0.12 wt.% SrO) whereas S-apatite (0.16–0.22 wt.% SrO) plots in the low Sr pole of the H-apatite compositional field (Tables 1, 2, Fig. 4). A plot of Sr-CaO shows a negative slope in H-apatite suggesting Sr–Ca substitution (Fig. 4a). Plots of Sr versus Mn and Y show a negative correlation in H-apatite (Fig. 4b and c). Yttrium concentration ranges from 0.02 to 119 ppm in H-apatite, from 40 and 283 ppm in S-apatite and from 14 to 2800 ppm in M-apatite. Total REE contents of H-apatite are generally low, ranging from 0.05 to 450 ppm, compared to those of

Table 1
Major (wt.%) and trace element (ppm) composition of representative hydrothermal (H) apatites.

Sample	LG9074	LG9132	LG9209	LG9079	LG9139	LG9115	BV5758	BV5752	BV5748	BV5756	NV1813	NV1805
Analysis	8	5	4	4	13		7	7	8		14	
Locality	Logrosán						Belvís				Navalmoral	
Type	Fibrous apatite			BSE-bright apatite	BSE-dark apatite		Fibrous apatite	BSE-bright apatite	BSE-dark apatite		Prismatic apatite	
				Patchy-zoned apatite				Concentric-zoned apatite				
P_2O_5	41.88	40.25	41.42	41.17	41.68	40.69	40.67	42.06	41.03	42.53	40.71	42.37
SiO_2	bdl	bdl	bdl	bdl	bdl	bdl	bdl	bdl	bdl	bdl	bdl	bdl
FeO	0.05	0.02	bdl	0.22	bdl	bdl	0.06	0.02	0.15	bdl	bdl	0.07
MnO	0.09	0.04	0.01	0.28	0.01	0.12	0.34	0.13	0.11	0.15	bdl	0.09
MgO	bdl	bdl	bdl	bdl	bdl	bdl	bdl	bdl	bdl	bdl	bdl	bdl
CaO	56.20	56.23	55.69	52.68	55.55	54.04	54.03	54.65	55.25	54.76	55.65	54.52
Na_2O	0.02	0.01	bdl	bdl	bdl	bdl	0.01	bdl	0.07	bdl	bdl	bdl
SrO[a]	0.33	0.38	0.30	3.85	0.40	1.42	1.12	1.14	0.12	0.85	0.32	0.39
F	3.36	3.90	3.36	3.65	3.57	3.78	3.57	3.59	3.55	3.57	3.45	3.40
Cl	0.02	0.01	bdl	bdl	0.01	bdl	bdl	bdl	bdl	0.02	bdl	bdl
Sum	101.95	100.84	100.78	101.84	101.21	100.05	99.80	101.59	100.28	101.87	100.13	100.84
F,Cl = −O	0.69	0.79	0.68	0.74	0.73	0.77	0.73	0.73	0.72	0.73	1.45	1.49
Total	101.26	100.05	100.10	101.10	100.48	99.28	98.07	100.08	99.56	101.14	98.82	99.35
Be	1.08	0.45	0.91	10	9.97	0.72	41	0.07	18	14	<0.88	<1.00
B	4.02	6.62	6.65	5.55	7.55	5.91	3.49	3.19	4.66	4.27	<6.32	<3.82
Sc	2.03	<0.87	3.33	0.87	1.19	<1.19	<1.07	<1.15	<3.95	<1.32	<0.43	<0.33
Sr[b]	2261	2248	2950	29455	3854	16567	3148	5059	1216	1209	7200	3060
Y	2.16	4.43	9.93	0.29	10	3.54	4.63	0.04	119	62	1.04	0.41
Zr	0.05	0.45	0.03	0.10	0.116	0.04	0.04	0.02	2.17	2.03	0.33	0.12
Nb	<0.01	0.09	<0.02	0.01	0.025	0.16	0.23	0.01	0.10	0.04	0.28	0.12
La	0.09	0.04	0.25	0.02	0.403	0.02	1.26	0.01	30	11	7.38	2.25
Ce	0.29	0.26	1.18	0.02	1.2	0.09	4.37	0.02	122	45	15	5.22
Pr	0.05	0.09	0.27	0.03	0.31	0.02	0.85	0.01	22	7.15	1.74	0.55
Nd	0.43	0.75	2.32	0.03	2.18	0.21	5.20	0.04	138	38	6.83	1.96
Sm	0.20	0.59	1.67	0.03	1.4	0.30	2.39	0.01	55	14	1.31	0.52
Eu	0.19	1.01	2.12	0.03	1.29	0.28	8.55	0.02	27	15	0.19	0.15
Gd	0.41	1.13	2.53	0.09	3	0.57	2.51	0.02	71	23.71	0.82	0.28
Tb	0.09	0.18	0.31	0.02	0.44	0.09	0.28	0.01	7.81	2.77	0.09	0.04
Dy	0.37	1.03	1.79	0.05	2.47	0.66	1.33	0.01	33	15	0.43	0.18
Ho	0.08	0.16	0.29	0.01	0.41	0.09	0.15	<0.01	4.74	2.15	0.04	<0.04
Er	0.17	0.37	0.73	0.03	0.78	0.25	0.31	0.01	7.98	4.43	<0.19	<0.13
Tm	0.01	0.04	0.08	<0.01	0.09	0.03	0.03	<0.01	0.69	0.51	<0.02	<0.02
Yb	0.12	0.2	0.62	0.02	0.55	0.22	0.17	<0.01	3.66	2.86	<0.12	<0.25
Lu	0.02	0.02	0.07	0.01	0.08	0.01	0.03	<0.01	0.38	0.39	<0.02	<0.04
Hf	<0.01	<0.01	<0.01	<0.01	0.01	<0.01	<0.01	<0.01	0.07	0.07	<0.14	<0.12
Ta	<0.00	<0.01	<0.03	<0.01	<0.01	<0.01	0.01	<0.01	<0.01	<0.01	<0.03	<0.04
Pb	0.04	0.43	0.22	0.59	0.087	2.81	0.83	0.27	3.39	1.41	6.90	2.92
Th	0.02	<0.01	<0.01	<0.01	0.01	<0.01	0.03	0.03	0.06	0.04	2.98	0.99
U	0.01	0.03	0.37	0.02	0.01	0.01	1.41	0.01	11	4.32	0.07	0.39

[a] EMP analysis.
[b] LA-ICP-MS analysis.

Table 2
Major (wt.%) and trace-element (ppm) composition of representative magmatic (M) apatites from Logrosán, Belvís, and Navalmoral granites and of apatites (S) in Neoproterozoic metasediments (Fontanarejo).

Sample	GRLOG1160	GRLOG6962	GRLOG7618	GRLOG7931	GRBELV1	GRBELV3	GRBELV6	GRNAV183	GRNAV202	FONT1	FONT2
Analysis	28				7			8		25	
Locality	Logrosán				Belvís			Navalmoral		Fontanarejo	
P_2O_5	43.00	42.06	42.09	43.31	41.43	41.85	41.86	40.48	42.09	41.27	42.09
SiO_2	bdl	0.04	0.02	0.01	bdl	bdl	bdl	bdl	bdl	bdl	bdl
FeO	0.61	0.26	0.61	0.92	1.41	1.40	1.12	0.27	0.35	0.08	0.35
MnO	1.35	0.49	1.14	0.75	2.96	2.80	2.52	0.39	0.53	bdl	0.53
MgO	0.01	bdl	bdl	bdl	0.07	0.09	0.03	bdl	bdl	0.03	bdl
CaO	53.53	54.47	53.70	54.11	51.33	51.54	51.59	54.64	55.38	55.60	55.38
Na_2O	0.02	0.01	bdl	0.02	0.12	0.14	0.13	0.14	0.13	bdl	0.13
SrO[a]	0.09	0.11	0.11	0.12	0.01	0.01	0.01	0.01	0.02	0.22	0.02
F	3.60	3.58	3.15	3.23	3.45	3.16	3.14	3.51	3.31	4.03	3.31
Cl	bdl	0.02	0.01	bdl	0.02	0.02	0.05	0.02	0.02	0.03	0.02
Sum	102.21	101.04	100.83	102.47	100.80	101.01	100.45	99.45	101.81	101.25	101.81
F,Cl = −O	1.52	1.51	1.33	1.36	1.46	1.34	1.33	1.48	1.40	1.70	1.40
Total	100.69	99.53	99.50	101.11	99.34	99.67	99.12	97.97	100.41	99.55	100.41
Be	0.32	0.72	0.05	<0.68	<3.12	<2.34	<2.21	<0.78	<0.53	4.58	<0.53
B	48.	6.18	7.37	5.04	<3.67	<2.51	<2.41	<4.84	5.86	12.9	5.86
Sc	1.37	0.85	2.68	1.63	14	3.28	2.48	1.17	1.17	3.26	1.17
Sr[b]	428	437	406	169	65	48	45	96	115	2300	115
Y	229	75	20	82	725	2749	1254	2230	2020	255	2020
Zr	1.34	<3.75	0.56	2.90	0.88	1.50	1.06	0.12	0.06	7.8	0.06
Nb	<0.01	0.10	<0.11	< 0.09	<0.36	<0.23	<0.24	<0.04	<0.02	0.22	<0.02
La	198	352	66	272	332	416	412	239	178	329	178
Ce	392	676	120	519	594	1020	818	815	682	680	682
Pr	41	71	12	53	77	173	116	135	112	69	112
Nd	147	258	49	182	302	901	483	657	548	243	548
Sm	31	44	11	35	87	345	150	249	221	46	221
Eu	61	48	17	34	17	13	15	10	12	16.5	12
Gd	25	26	8.70	25	92	440	156	318	271	43.3	271
Tb	4.33	2.93	1.16	3.25	21	92	37	58	51	6.54	51
Dy	30	14	5.60	15	116	538	228	382	347	42	347
Ho	5.46	2.14	0.66	2.02	18	83	32	74	64	8.49	64
Er	17	5.78	1.60	4.62	44	186	77	198	175	25	175
Tm	3.00	0.90	0.19	0.62	6.27	22	11	27	26	3.4	26
Yb	21	7.00	1.62	4.67	43	138	78	165	161	19.1	161
Lu	2.91	0.94	0.16	0.60	4.87	16	9.25	21	20	2.4	20
Hf	0.03	<0.25	<0.01	0.08	<1.61	<1.09	<1.03	0.06	0.09	0.13	0.09
Ta	<0.01	0.02	<0.01	<0.01	<0.31	<0.27	<0.27	0.01	0.02	0.01	0.02
Pb	57	27	59	43	6.35	7.54	7.38	8.64	8.52	21	8.52
Th	17	40	14	22	10	4.82	8.61	1.17	1.0	45	1.0
U	69	34	47	164	266	297	316	99.3	127	36	127

[a] EMP analysis.
[b] LA-ICP-MS analysis.

M-apatite and S-apatite, whose values vary from 600 to 7800 ppm and from 100 to 1500 ppm, respectively. There is no significant difference in total REE contents between the Logrosán, Belvís and Navalmoral H-apatites (Fig. 4d).

Th and U contents in H-apatite are low, b8 ppm and b12 ppm, respectively, in contrast to M- and S-apatites, that show variable amounts of Th (1–800 ppm) and U (16 to 800) (Fig. 5a). High Th contents could be recognized in the Logrosán magmatic apatite (Fig. 5a). A positive slope for Th–U and for Th–Ce is observed for M-, H- and S-apatites (Fig. 5a and b).

Chondrite-normalized REE patterns of representative H-, M- and S-apatites are shown in Fig. 6a and b. The Navalmoral H-apatite presents a REE pattern different from that of the other hydrothermal apatites. It shows a LREE-enriched trend with a slightly negative Eu anomaly and HREE below detection limits (Table 1). The other hydrothermal apatites (Belvís and Logrosán) mainly show concave downwards REE patterns with variable positive Eu anomalies (most Eu/Eu* = 1–4 and Eu/Eu* = 1–9, respectively) (Fig. 6a).

Magmatic apatites show more flat REE patterns than H-types and tend to have prominent negative Eu anomalies with Eu/Eu* values between 0.05 and 0.6 (Figs. 5d a n d 6b) excepting the Logrosán granite ap-atite which shows a marked positive Eu/Eu* anomaly and certain degree of REE fractionation with $(Ce/Yb)_n$ values above 1 (Figs. 5c a n d 6b).

Metamorphic S-apatites show flat patterns with slight negative Eu anomalies (Fig. 6b).

H-apatite is often zoned. Different compositions between H-apatite types (e.g. fibrous, prismatic, patchy-zoned or concentric-zoned) have been detected (Table 1). The zonation has been studied using back-scattered electron images (Fig. 7). Concentrically-zoned apatite is characteristic from the Belvís veins and patchy-zoned apatite from the Logrosán veins. No zoning has been detected in Navalmoral H-apatite. Total REE contents range between 0.1 and 184 ppm in concentrically-zoned apatite, and between 0.3 and 5.5 ppm in irregularly zoned crystals. In both cases the REE-richest parts correspond to BSE-dark apatite (Fig. 7a, b analyses no. 51, 53, 54 and Fig. 7c, d, analyses 77, 79) while BSE-bright zones have the lowest REE values (Fig. 7a, b analyses no. 52, 55, 56, and Fig. 7c, d, analyses 76, 78). The chondrite-normalized REE pat-terns of the dark and bright areas show HREE depletion in concentrically-zoned apatite compared to patchy-zoned apatite (Fig. 6a). Magmatic and metasedimentary apatites are not significantly zoned.

5.2. Sulfide composition

Average compositions of arsenopyrite, pyrite and chalcopyrite from the Logrosán veins are given in Table 3. Arsenopyrite is very scarce in the hydrothermal veins and only some grains coexisting directly with

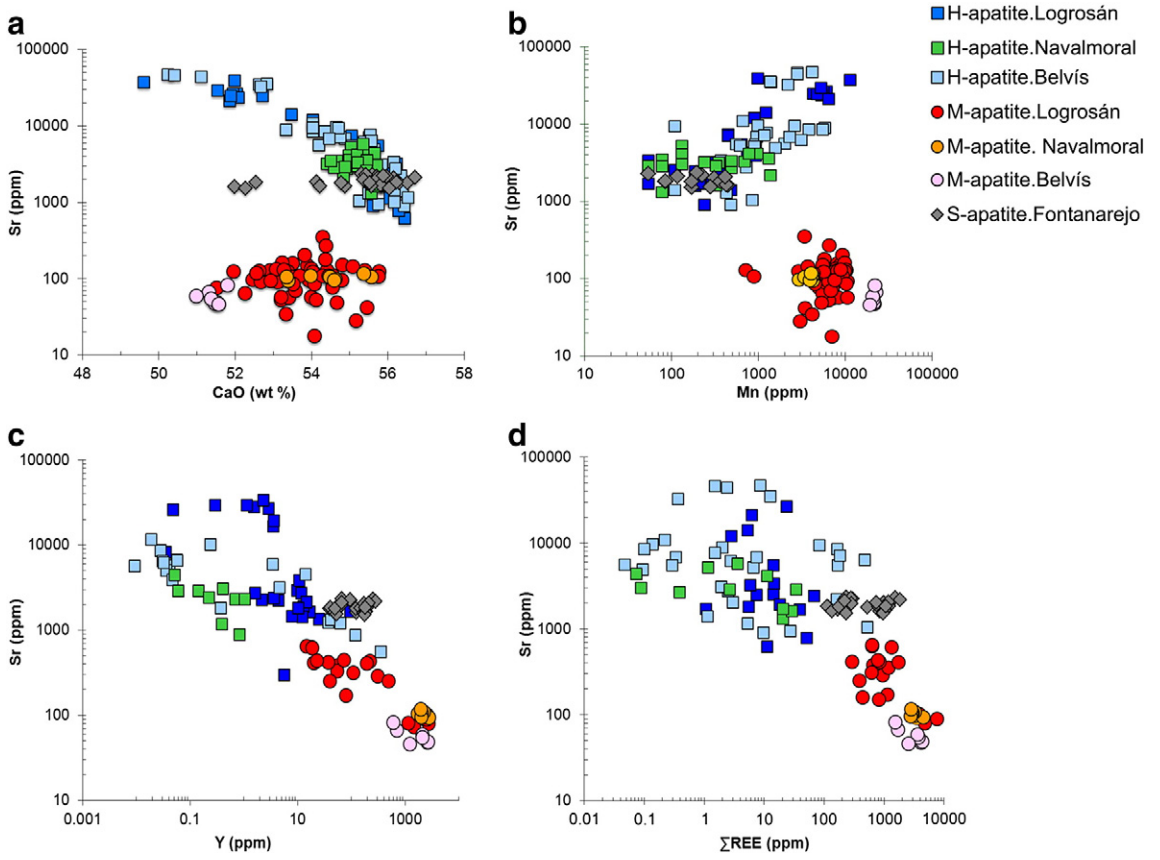

Fig. 4. Trace element composition of hydrothermal (H), magmatic (M) and sedimentary (S) apatites: (a) Sr vs. CaO; (b) Sr vs. Mn; (c) Sr vs. Y; (d) Sr vs. total REEs.

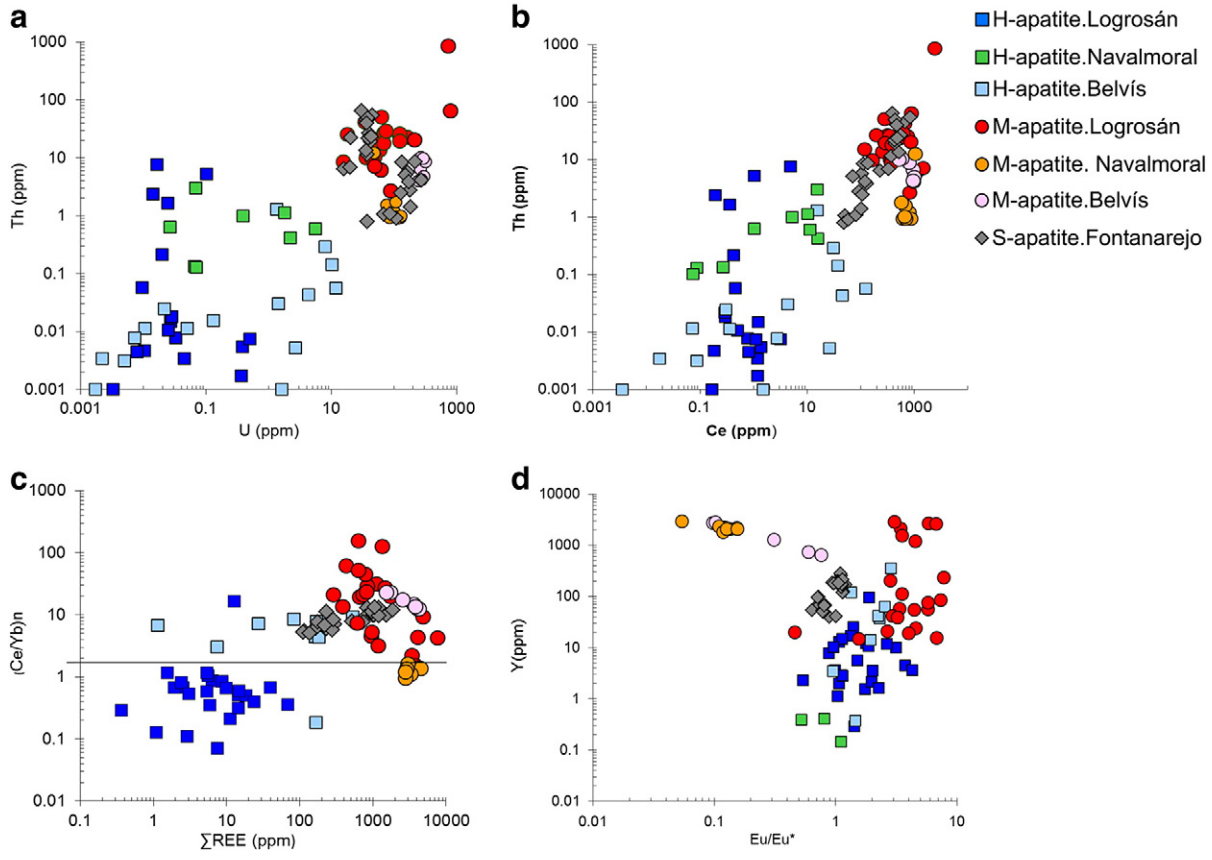

Fig. 5. Trace element composition of hydrothermal, magmatic and metasedimentary apatites: (a) Th vs. Ce; (b) Pb vs. U; (c) (Ce/Yb)cn vs. total REEs; (d) Y vs. Eu/Eu*.

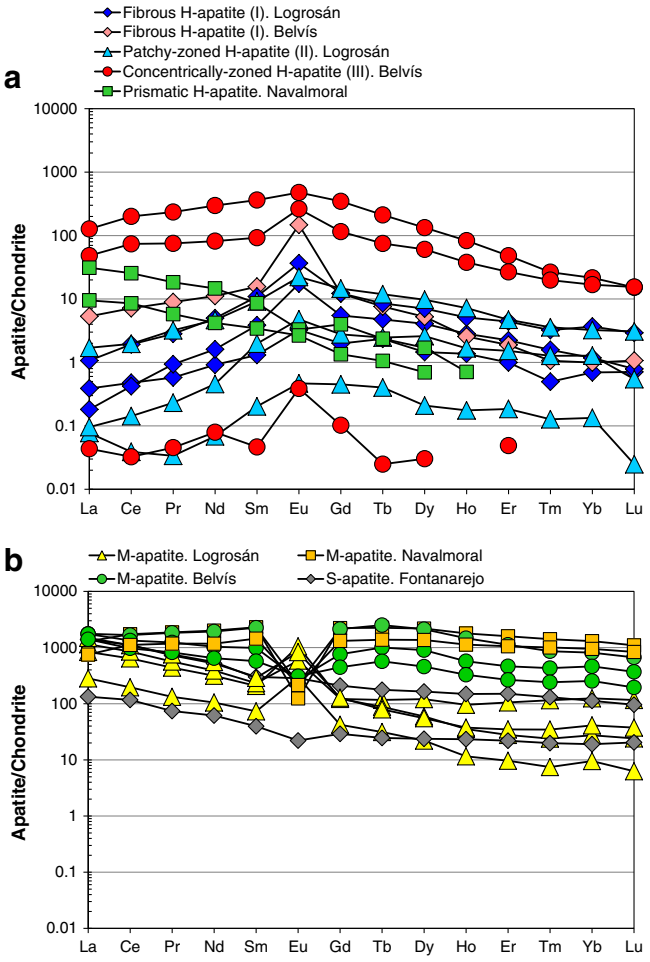

Fig. 6. Chondrite-normalized REE patterns of apatite. Normalizing values from McDonough and Sun (1995). (a) Hydrothermal apatite and (b) magmatic apatite. Data from Tables 1 and 2.

pyrite have been found in the margin of the Logrosán veins. Most of the arsenopyrite crystals are homogeneous or slightly zoned. Arsenopyrite grains showing N1 at.% As variation from core to the rim were rejected for geothermometry. The As content ranges between 43.5 and 44.3 wt.% and the Fe content is almost constant, around 35 wt.%. Total concentration of Bi, Ag, Mn, Ni, Cd, Pb, Cu, Sn, Zn and Sb is small and does not exceed 0.4 wt.% (Table 3).

5.3. Fluid inclusion data

Quartz–apatite veins are devoid of good material for fluid inclusion studies. The quartz-hosted fluid inclusions were mostly too small (b3 μm) for quantitative investigation and fibrous apatite, "dahllite", lacked clarity to identify the fluid inclusions. Suitable fluid inclusions for microthermometry analysis were found only in apatite III crystals from the Belvís veins and in quartz from the Navalmoral and Logrosán quartz–apatite veins. Microthermometric data are summarized in Table 4 with all abbreviations used in the text.

Three types of fluid inclusions have been observed in hexagonal crystals of apatite from the Belvís veins: primary, pseudosecondary and secondary inclusions. Primary and pseudosecondary fluid inclu-sions are two phase (L + V) with the vapor phase comprising 5% to 10% of inclusion volume. Both types of inclusions are b5 t o 4 0 μm i n size. Equidimensional fluid inclusions distributed along growth planes, parallel to crystal faces (Fig. 8a and b) have been considered as primary. Secondary one-phase fluid inclusions (b5 t o 5 0 μm) are scattered along healed fractures displaying irregular shapes and commonly show evidence for stretching and necking-down. Two fluid inclusion types, primary and secondary, have been identified in quartz from the Navalmoral and Logrosán veins (Table 4). Fluid inclusions are biphasic and dominantly liquid (L) with a minor vapor (V) phase, 5–10%, except primary fluid inclusions in quartz of Logrosán (5–40%). They are all s m a l l i n s i z e (b5 t o 1 5 μm).

In apatite, primary and secondary fluid inclusions show the first melting temperature (T_e) at about −21 °C, and this corresponds to eutectic melting temperatures in the H_2O–NaCl system and suggests that other salt species are not present in significant concentrations. Primary fluid inclusions display temperatures of final ice melting ($T_m$ice) that range from −0.1 to −4.1 °C, corresponding to salinities between 0.2 and 6.7 wt.% NaCl equiv. Homogenization temperature (T_h) occurs in the liquid phase at temperatures between 125 and 165 °C. The final ice melting temperature ($T_m$ice) was between −0.5 and −1.6 °C in pseudosecondary fluid inclusions, corresponding to salinities ranging from 0.9 and 2.7 wt.% NaCl equiv. Homogenization in the liquid phase at temperatures (T_h) between 115 and 140 °C was observed (Fig. 9).

In quartz, fluid inclusions also display the first melting temperature (T_e) a t a b o u t −21 °C, indicating the predominance of NaCl among dis-solved salts. The temperature of final ice melting ($T_m$ice) in primary fluid inclusions ranges from −0.1 to −0.8 °C which corresponds to salinities between 0.2 and 1.4 wt.% NaCl equiv. and from −0.2 and−0.5 °C for secondary fluid inclusions, corresponding to 0.4–0.9 wt.%NaCl equiv. Primary fluid inclusions homogenize into liquid phase (T_h) from 225 to 250 °C in quartz from Navalmoral and between 150 and 350 °C in quartz from Logrosán. Secondary fluid inclusions show T_h ranging between 110 and 235 °C (Table 4).

5.4. Stable isotope data

The $\delta^{18}O_{SMOW}$ values for hydrothermal quartz in Logrosán (+13.8 to +16.7‰) are similar to the $\delta^{18}O_{SMOW}$ of the nearby granite (+14.1 to +15.0‰) (Table 5, Fig. 10). Nevertheless, dolomite found in the quartz–apatite veins has a $\delta^{18}O_{SMOW}$ value of 20.8‰ (and a $\delta^{13}C_{PDB}$ of −8.5‰) in the same range of hydrothermal dolomite phases (D_3 and D_4) affecting Ediacaran carbonate rocks of the Ibor Group of the SGC (Herrero et al., 2011).

Hydrothermal quartz in the Navalmoral veins is isotopically lighter, with $\delta^{18}O_{SMOW}$ values ranging between + 11.4 and + 13.3‰. Navalmoral results are more comparable to $\delta^{18}O_{SMOW}$ values measured in metasedimentary rocks of this study in the central sector of the SGC (13.1–13.4‰) (Table 5, Fig. 10) and to other $\delta^{18}O$ values given by other authors in the same area (ranging from +11.6 to +15.7‰, a f t e r Ugidos et al., 1997).

6. Discussion

6.1. Nature of the hydrothermal fluids

The source of the ore-forming hydrothermal fluids, whether related to magmatic system or fluids of unknown origin equilibrated with granites or with Neoproterozoic metasedimentary sequences, is the main subject of debate in this study. H- and M-apatites show significant differences in their chemistry. Sr enrichment, Mn–Y–REE–Th–U–Pb depletion, convex-up chondrite-normalized REE pattern and positive Eu anomalies indicate different sources for H- and M-apatite formation. The high Sr content and the Mn–Y–REE–Th–U–Pb depletion (Figs. 4 and 5b) of H-apatite (Logrosán, Belvís–Navalmoral) suggest different sources for H- and M-apatite formation. Sr (b500 ppm), Mn (10^3–10^4) and Y (10–10^3) contents in magmatic apatite are very similar to those of other granitoids, indicating the partitioning of Sr into plagioclase (Belousova et al., 2002). H-apatites from Logrosán, Belvís and Navalmoral show SrO ranging between 0.3 and 1.4 wt.% SrO. This high Sr content could have been incorporated during the circulation of the ore-forming fluids through phosphate occurrences in Neoproterozoic

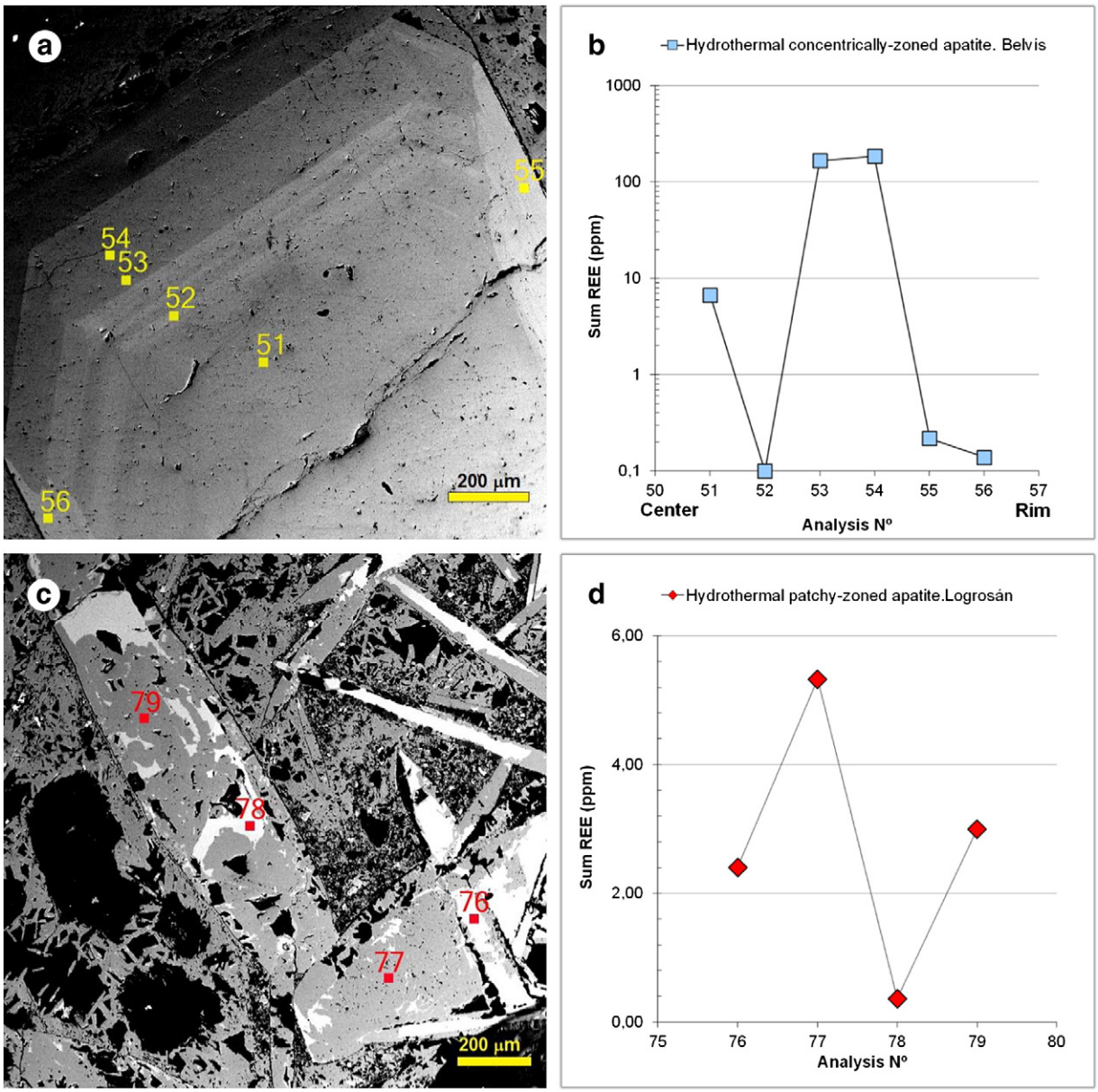

Fig. 7. Backscattered electron images of hydrothermal (H-type) apatite: (a) Concentrically zoned apatite crystal from the Belvís vein. (b) Changes in total REE concentration along a traverse from BSE-dark and BSE-bright areas (Belvís vein). (c) Patchy-zoned apatite from the Logrosán vein. (d) Changes in total REE concentration in BSE-dark and BSE-bright areas (Logrosán vein).

sediments (S-apatite: 0.16–0.22 wt.% SrO) or through certain carbonate beds. The Ediacaran carbonate unit (Ibor Group in Fig. 1), close to the Belvís and Navalmoral quartz–apatite veins, includes dolomite with Sr up to 0.5 wt.% (Herrero et al., 2011). In addition, chondrite-normalized REE patterns show convex-up shape for most of the H-apatites, in contrast with the almost flat REE patterns of the granitic M-apatites. Positive Eu anomalies (Eu^{2+}) in H-apatites indicate reducing conditions, while negative Eu anomalies (Eu^{3+}) in the M-apatites from the Belvís and Navalmoral granites point at oxidizing conditions and marked feld-spar fractionation. The origin of positive Eu anomalies in the M-apatite of the Logrosán granite could be related to variable redox conditions, to compositional heterogeneities in the felsic magma or to the influence of co-crystallization of other magmatic phases (Chu et al., 2009).

An attempt was made to determine the ore-forming conditions combining the arsenopyrite geothermometry with fluid inclusion data. The ore-forming fluids show a simple cooling (T_h from 350 to 110 °C) of low salinity fluids (0.2 and 1.4 wt.% NaCl equiv.) in the Logrosán and Navalmoral veins (Fig. 9). On the other hand, aqueous fluids trapped in the Belvís apatite have low to moderate salinities (0.2 and 6.7 wt.% NaCl equiv.) at lower temperature (T_h: 125 to 165 °C), showing a dilution process. Because of his refractory nature, arsenopyrite compo-sition reflects formation temperature (Kretschmar and Scott, 1976). Although the arsenopyrite geothermometer should be used with caution (Kerestedjian, 1997; Sharp et al., 1985), it could provide an estimate of formation temperatures in conjunction with fluid inclusion and geologi-cal data. The arsenopyrite geothermometer for ore deposits formed at temperatures higher than 300 °C was proposed by Kretschmar and Scott (1976) and re-examined by Sharp et al. (1985). The average compo-sition of arsenopyrite from the Logrosán veins clusters at 32.07–32.5 at.%As that corresponds to temperatures of 440 ± 10 °C, close to the maxi-mum T values estimated with fluid inclusion data. The estimated medium-to-low temperature of ore formation suggests that the hydro-thermal fluids could not be directly related either to granite intrusion or even to the fast cooling of these small and shallow felsic plutons.

In summary, the source of the hydrothermal ore-forming fluids is problematic. Nonetheless, the most similar apatite chemical composition

Table 3
Average composition of sulfide minerals from Logrosán veins (Apy: arsenopyrite, Py: pyrite, Ccp: chalcopyrite).

Sample	LG3543	LG3545	LOG3545	
Mineral	Apy		Py	Ccp
Analysis	8	10	11	6
As wt.%	44.27	43.55	0.83	0.83
Fe	35.47	35.44	46.31	46.31
Bi	0.39	0.28	0.09	0.09
S	18.57	18.76	51.29	51.29
Co	0.31	0.23	0.05	0.05
Ag	0.01	0.03	0.01	0.01
Mn	0.04	0.04	0.03	0.03
Ni	0.23	0.24	0.01	0.01
Cd	0.01	<0.01	0.03	0.03
Pb	0.14	0.14	0.27	0.27
Cu	<0.02	<0.02	<0.02	<0.02
Zn	0.01	<0.01	0.01	0.01
Sb	0.06	0.09	0.04	0.04
Total	99.49	98.80	98.74	98.74
As at.%	32.49	32.07	0.45	0.00
Fe	34.93	35.00	33.93	24.93
Bi	0.10	0.08	0.02	0.02
S	31.85	32.28	65.45	50.41
Co	0.29	0.22	0.04	0.02
Ag	0.00	0.01	0.00	0.01
Mn	0.04	0.04	0.02	0.00
Ni	0.22	0.23	0.01	0.00
Cd	0.00	0.00	0.01	0.00
Pb	0.04	0.04	0.05	0.05
Cu	0.00	0.00	0.00	24.42
Zn	0.01	0.00	0.01	0.01
Sb	0.03	0.04	0.01	0.01

between hydrothermal and sedimentary types suggests a greater genetic proximity between them. Moreover, the good overlap of the oxygen isotopic signatures of hydrothermal dolomite data from the Logrosán quartz–apatite vein with those of hydrothermally altered carbonate beds of the SGC (Fig. 10) allows us to suggest a model involving the circulation of ore fluids mostly permeating through the surrounding metasedimentary country rocks.

6.2. The question of the age of the P-rich veins

The extremely low U and Th contents shown by the hydrothermal apatites (mostly below 0.6 ppm, Table 1) made impossible to date these phosphates by conventional U–Pb methods, including fission tracks. Moreover, the absence of associated phyllosilicates or other accessory minerals (e.g., zircon, monazite) contributed to the failure in geochronological dating.

Hydrothermal activity in central Spain has been related to three main stages yet not well geochronologically constrained (Galindo et al., 2010; Martín-Crespo et al., 2002; Tornos et al., 2000): (1) mineralizations related to the end of the Variscan magmatic activity and the initiation of proto-rifting with scarce alkaline intrusions

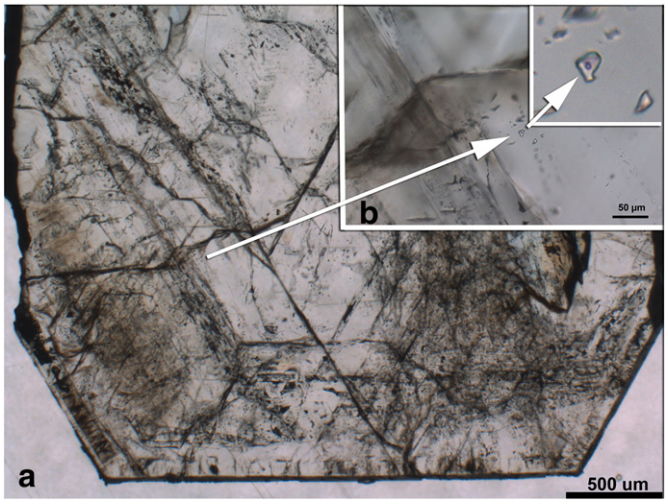

Fig. 8. Fluid inclusions in apatite: (a) Primary fluid inclusions oriented along a crystal growth band (b) detail of an equidimensional fluid inclusion.

(293–255 Ma); (2) hydrothermal activity starting from the Early Jurassic tholeiitic rifting, related to the Atlantic opening and giving rise to F–Ba–Pb–Zn ore veins in many places of the CIZ (201–120 Ma), including the nearby Toledo shear zone (Villaseca et al., 2005);(3) minor hydrothermal activity and alteration related to the Cretaceous–Tertiary boundary (75–50 Ma), also identified by apatite fission-track analyses in granitic and metamorphic rocks of the Montes de Toledo area but related to low-T fluids (≤80 °C after Barbero et al., 2005). A scarce mantle-derived alkaline magmatic activity from 103 to 69 Ma has been recorded dispersedly within the Iberian microplate: Portugal (Grange et al., 2010), Galicia (Ancochea et al., 1992), Basque country and Catalonian coastal Range (Ubide, 2013).

Although more work needs to be made, the moderate-T hydrother-mal activity described in the studied P-rich veins (up to 350–440 °C), in agreement with dolomitization processes in carbonate rocks of the SGC (up to 500 °C, Herrero et al., 2011), suggests that the ore studied cannot be related to the Cretaceous–Tertiary low-T activity of the area. The great isotopic similarity and T conditions between carbonates of the studied veins and the dolomitization events in carbonate metasediments of the SGC make a more probable Mesozoic age for their formation. We propose the disconnection of this hydrothermal activity from the granite intrusion timing. This hypothesis is based on the lack of clear petrogenet-ic relationship of the studied P-rich veins with the associated granitoids, as suggested by the contrasted chemical composition between M- and H-apatite types, and on the absence of spatial relationship of granitoids with the hydrothermal dolomitization processes of carbonate rocks of the SGC. Small granite intrusions (e.g., Logrosán and Belvís) necessarily lose heat quickly in such epizonal environments (the SGC) and hence they lack effective time to generate significant convective hydrothermal cells. This important issue needs to be confirmed by future accurate geo-chronological data.

Table 4
Microthermometric data from fluid inclusions recognized in apatite and quartz; $T_m$ice: last ice melting; T_h: homogenization to vapor (V) or liquid (L); N: number of measurements. P, PS and S are primary, pseudosecondary and secondary inclusions respectively.

Location	Mineral host	Inclusion generation	N	Physical state	Vapor (%)	$T_m$ice (ºC)	T_h (ºC)	Salinity (wt.% NaCl equiv.)
Belvís	Apatite	P	20	Two-phase	5–10	−0.1/−4.1	125/165L	0.2/6.7
	Apatite	PS	20	Two-phase	5–10	−0.5/−1.6	115/140L	0.9/2.7
	Apatite	S		One-phase				
Navalmoral	Quartz	P	12	Two-phase	5–10	−0.2/−0.8	225/250L	0.4/1.4
	Quartz	S	5	Two-phase	5–10	−0.3/−0.5	110/120L	0.5/0.9
Logrosán	Quartz	P	10	Two-phase	5–40	−0.1/−0.8	150/350L	0.2/1.4
	Quartz	S	5	Two-phase	5–10	−0.2/−0.3	140/235L	0.4/0.5

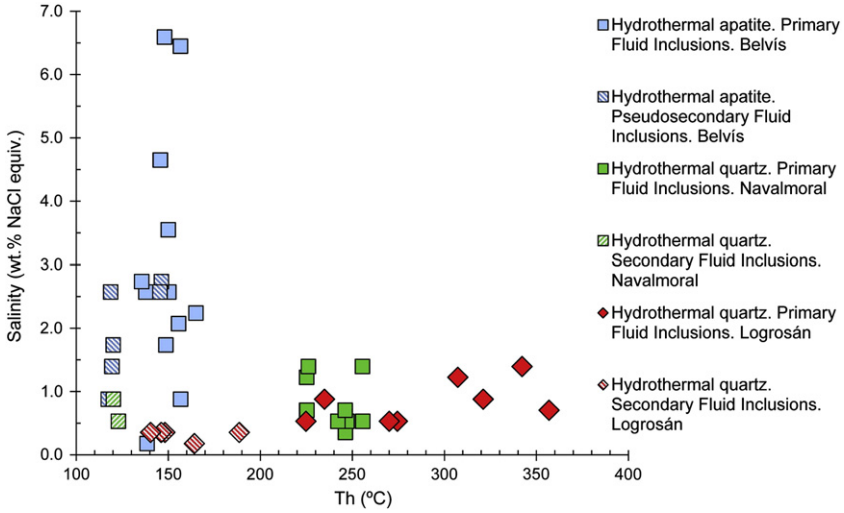

Fig. 9. Plot showing homogenization temperature (Th) versus salinity (wt.% NaCl equiv.).

6.3. The southern CIZ as a phosphorous-rich domain

The presence of disperse phosphate rocks and even of phosphorite deposits within the lithostratigraphic units of the SGC is largely known (e.g., Gabaldón López et al., 1986; Perconig et al., 1986), but even more remarkable is the contrasted geochemical features between metasedimentary rocks from this southern part of the CIZ in comparison with those from the northern CIZ. The metasedimentary rocks of the southern CIZ are on average richer in P than those of the northern part (Villaseca et al., 2014), thus defining a P-rich Neoproterozoic sedimen-tary realm.

It is noteworthy that most of the perphosphorous Variscan granites described in the Iberian belt are restricted to this southern domain of the CIZ (Villaseca, 2011; Villaseca et al., 2008). These P-rich plutons suggest granite derivation from pelitic and greywacke sources isotopically similar to those of the SGC (e.g., Antunes et al., 2008; Menéndez and Bea, 2004; Ramírez and Menéndez, 1999; Villaseca et al., 2008), attesting to a major crustal recycling of those P-rich metasediments during the Variscan orogeny.

The studied phosphorous rich veins would represent a second event of recycling of metasediments (in principle from the SGC) within the southern CIZ during post-Variscan hydrothermal fluid circulation, which would give rise to the only known quartz–apatite veins in Western Europe. The intense geochemical reworking of original P-rich metasediments during partial melting or hydrothermal events could originate these rare P-rich ore mineralizations suitably called as "Iberian-type" (Aizpurúa et al., 1982).

Table 5
Oxygen isotope data for hydrothermal ores and whole rocks (granite and SGC rocks).

Location	Sample	Mineral/whole rock	$\delta^{18}O$ (‰ SMOW)
Logrosán vein	MC	Quartz	15.5
	MC	Quartz	15.9
	MC3C	Quartz	16.7
	MC4	Quartz	15.1
	COS13	Quartz	14.2
	COS13	Quartz	13.8
	MC3A	Dolomite	20.8
Logrosán granite	LF4044	Granite	15.0
	LF4045	Granite	14.1
	LF4048	Granite	14.5
SGC	LF4046	SGC	13.1
	LF4043	SGC	13.2
	LF4047	SGC	13.4
Navalmoral vein	P1A	Quartz	11.6
	P3	Quartz	11.4
	P4	Quartz	13.3
	P1	Quartz	12.2

7. Conclusions

Hydrothermal quartz–apatite veins of Extremadura constitute a distinctive type of ore deposit which occurs exclusively in the southern Central Iberian Zone. Hydrothermal and magmatic apatites show markedly different chemical composition. The Sr-rich character of H-apatite may be inherited from phosphate and carbonate levels within the Neoproterozoic metasediments. REE, fluid inclusion and stable isotope data are consistent with a long lasting hydrothermal activity. Extensive fluid circulation would have taken place along extension faults, breccias and stockworks, mostly interacting with phosphate and carbonate beds of the Neoproterozoic Schist–Greywacke Complex. Mineral precipitation was then controlled by cooling and dilution of aqueous low-salinity fluids allowing the formation of the quartz–apatite ores. The importance of this "Iberian-type" hydrothermal veins merits future detailed and accurate geochronological work.

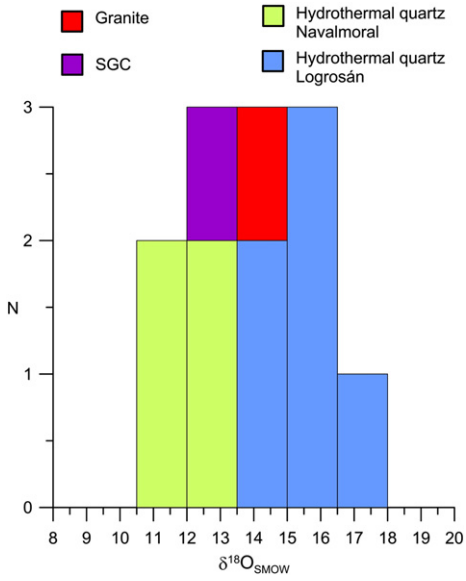

Fig. 10. Histogram of $\delta^{18}O_{SMOW}$ values for quartz from hydrothermal veins, granites and metasediments from the SGC.

Acknowledgments

This study has been carried out with the support of the projects CGL2012-32822 (Ministerio de Economía y Competitividad of Spain) and 910492 (Complutense University of Madrid). The authors thank Ester Boixereu and Cecilia Pérez-Soba for their suggestions and helpful comments. Sonia García de Madinabeitia, Alfredo Larios and Clemente Recio are thanked for their technical support with LA-ICP-MS, EMPA and stable isotope analysis, respectively. E. Chicharro would like to thank Dr. Teresa E. Jeffries for the opportunity to undertake the ana-lytical work in the Natural History Museum of London and for her assis-tance with the laser ablation technique. The authors thank the helpful comments and suggestions from two anonymous reviewers which improved the original manuscript.

References

Ábalos, B., Gil Ibarguchi, J.I., Sánchez-Lorda, M.E., Paquette, J.L., 2012. African/Amazonian Proterozoic correlations of Iberia: a detrital zircon U–Pb study of early Cambrian conglomerates from the Sierra de la Demanda (northern Spain). Tectonics 31 (3), TC3003. http://dx.doi.org/10.1029/2011TC003041.

Aizpurúa, J., Gumiel, P., Pineda, A., 1982. Introducción al estudio de los yacimientos de fosfatos del Macizo Ibérico meridional. Bol. Geol. Min. 93, 390–414.

Ancochea, E., Huertas, M.J., Ibarrola, E., Snelling, N., 1992. Diques basálticos en las proximidades de Orense. Evidencia de actividad magmática Cretácica en el noroeste de la península Ibérica. Rev. Soc. Geol. Esp. 5, 65–71.

Antunes, I., Neiva, A., Silva, M., Corfu, F., 2008. Geochemistry of S-type granitic rocks from the reversely zoned Castelo Branco pluton (central Portugal). Lithos 103, 445–465. http://dx.doi.org/10.1016/j.lithos.2007.10.003.

Barbero, L., Glasmacher, U.A., Villaseca, C., López-García, J.A., Martín-Romera, C., 2005. Long-term thermo-tectonic evolution of the Montes de Toledo area (Central Hercynian Belt, Spain): constraints from apatite fission-track analysis. Int. Earth Sci. 94, 193–203. http://dx.doi.org/10.1007/s00531-004-0455-y.

Belousova, E.A., Griffin, W.L., O'Reilly, S.Y., Fisher, N.I., 2002. Apatite as an indicator mineral for mineral exploration: trace-element compositions and their relationship to host rock type. J. Geochem. Explor. 76, 42–69. http://dx.doi.org/10.1016/S0375-6742(02) 00204-2.

Bodnar, T.S., 1993. Revised equation and table for determining the freezing point depression of H_2O–NaCl solutions. Geochim. Cosmochim. Acta 57, 683–684. http://dx.doi.org/10.1016/0016-7037(93)90378-A.

Boixereu, E., 2003. Historia y patrimonio minero de Logrosán (Cáceres). La mina de fosforita de La Costanaza. Cuad. Museo Geominero 2, 169–176.

Boixereu, E., 2004. Mina de fosfato de Logrosán, Cáceres. Tierra Tecnol. 26, 26–34.

Borthwick, J., Harmon, R.S., 1982. A note regarding ClF_3 as an alternative to BrF_5 for oxygen isotope analysis. Geochim. Cosmochim. Acta 46, 1665–1668. http://dx.doi.org/10.1016/0016-7037(82)90321-0.

Castro, A., 1985. The Central Extremadura Batholith — geotectonic implications (European Hercynian Belt) — an outlet. Tectonophysics 120, 57–68. http://dx.doi.org/10.1016/0040-1951(85)90086-1.

Chicharro, E., Villaseca, C., Valverde-Vaquero, P., Belousova, E., López-García, J.Á., 2013. U–Pb geochronology and source constraints for late S-type Variscan magmatism related to Sn–W metallogeny: the Logrosán granite pluton (Central Iberian Zone). Mineral. Mag. 77 (5), 874.

Chicharro, E., Villaseca, C., Valverde-Vaquero, P., Belousova, E., López-García, J.A., et al., 2014. Zircon U–Pb and Hf isotopic constraints on the genesis of a post-kinematic S-type Variscan tin granite: the Logrosán cupola (Central Iberian Zone). J. Iber. Geol. (accepted for publication).

Chu, M.-F., Wang, K.-L., Griffin, W.L., Chung, S.-L., O'Reilly, S.Y., Pearson, N.J., Iizuka, Y., 2009. Apatite composition: tracing petrogenetic processes in Transhimalayan granit-oids. J. Petrol. 50, 1829–1855. http://dx.doi.org/10.1093/petrology/egp054doi:10. 1093/petrology/egp054.

Clayton, R.N., Mayeda, T.K., 1963. The use of bromine pentafluoride in the extraction of oxygen from oxides and silicates for isotopic analysis. Geochim. Cosmochim. Acta 27, 43–52. http://dx.doi.org/10.1016/0016-7037(63)90071-1.

Dias, G., Leterrier, J., Mendes, A., Simões, P.P., Bertrand, J.M., 1998. U–Pb zircon and monazite geochronology of post-collisional Hercynian granitoids from the Central Iberian Zone (Northern Portugal). Lithos 45, 349–369. http://dx.doi.org/10.1016/S0024-4937(98)00039-5.

Gabaldón López, V., Hernández Urroz, S., Lorenzo Álvarez, S., Picart Boira, J., Santamaría Casavovas, J., Solé Pont, F.J., 1986. Sedimentary facies and stratigraphy of Precambrian–Cambrian phosphorite on the Valdecasa Anticline, Central Iberian Zone, Spain. In: Notholt, A.J.G., Sheldon, R.P., Davidson, D.F. (Eds.), Phosphate Deposits of the World 2. Cambridge University Press, Cambridge, pp. 422–428.

Galindo, C., Casquet, C., Tornos, F., 2010. Actividad paleo-hidrotermal episódica en la Sierra de Guadarrama (Sistema Central Español): nuevas edades K-Ar y correlación tectónica con la Cordillera Ibérica. Geogaceta 48, 159–162.

García de Madinabeitia, S., Roda-Robles, E., Pesquera, A., Sánchez, M.E., Gil Ibarguchi, J.I., 2013. Characterization of complex Fe–Mn phosphates by LA-ICP-MS methods. Mineral. Mag. 77, 1142.

Grange, M., Scharer, U., Merle, R., Girardeau, J., Cornen, G., 2010. Plume–lithospheric interaction during migration of Cretaceous alkaline magmatism in SW Portugal: evidence from U–Pb ages and Pb–Sr–Hf isotopes. J. Petrol. 51, 1143–1170.

Herrero, M.J., Martín-Pérez, A., Alonso-Zarza, A.M., Gil-Peña, I., Meléndez, A., Martín-García, R., 2011. Petrography and geochemistry of the magnesites and dolostones of the Edi-acaran Ibor Group (635 to 542 Ma), Western Spain: evidences of their hydrothermal origin. Sediment. Geol. 240, 71–84. http://dx.doi.org/10.1016/j.sedgeo.2011.08.007.

Jackson, S.E., Pearson, N.J., Griffin, W.L., Belousova, E.A., 2004. The application of laser ablation-inductively coupled plasma-mass spectrometry to in situ U–Pb zircon geochronology. Chem. Geol. 211, 47–69. http://dx.doi.org/10.1016/j.chemgeo.2004.06.017.

Jeffries, T.E., 2001. Elemental analysis by laser ablation ICP-MS. In: Alfassi, Z. (Ed.), Non-Destructive Elemental Analysis. Blackwell Science, Oxford, pp. 115–150.

Jochum, K.P., Weis, U., Stoll, B., Kuzmin, D., Yang, Q., Raczek, I., Jabob, D.E., Stracke, A., Birbaum, K., Frick, D.A., Günther, D., Enzweiler, J., 2011. Determination of reference values for NIST SRM 610–617 glasses following ISO guidelines. Geostand. Geoanal. Res. 35, 397–429. http://dx.doi.org/10.1111/j.1751-908X.2011.00120.

Julivert, M., Fontboté, J.M., Ribeiro, A., Conde, L.E., 1974. Memoria explicativa del Mapa tectónico de la Península Ibérica y Baleares. E: 1:1.000.000. Inst. Geol. Min. España, Madrid.

Kerestedjian, T., 1997. Chemical and morphological features of arsenopyrite, concerning its use a geothermometer. Miner. Petrol. 60, 231–243. http://dx.doi.org/10.1007/BF01173710.

Kretschmar, U., Scott, S.D., 1976. Phase relations involving arsenopyrite in the system Fe–As–S and their application. Can. Mineral. 14, 364–386.

Locutura, J. and Alcalde C. (Eds.), 2007. Mapa Metalogenético de Extremadura a escala 1: 250.000. Junta de Extremadura. Inst. Geol. Min. España, Madrid.

Martín-Crespo, T., Delgado, A., Vindel, E., López-García, J.A., Fabre, C., 2002. The latest Post-Variscan fluids in the Spanish Central System: evidence from fluid inclusion and stable isotope data. Mar. Petrol. Geol. 19, 323–337. http://dx.doi.org/10.1016/S0264-8172(02)00020-X.

McCrea, J.M., 1950. On the isotopic chemistry of carbonates and a paleotemperature scale. J. Chem. Phys. 18, 849–857. http://dx.doi.org/10.1063/1.1747785.

McDonough, W.F., Sun, S., 1995. The composition of the Earth. Chem. Geol. 120, 223–253. http://dx.doi.org/10.1016/0009-2541(94)00140-4.

Menéndez, L.G., Bea, F., 2004. El batolito Nisa-Alburquerque. In: Vera, J.A. (Ed.), Geología de España. IGME-SGE, Madrid, pp. 120–122.

Merino, E., Villaseca, C., Orejana, D., Jeffries, T., 2013. Gahnite, chrysoberyl and beryl co-occurrences as accessory minerals in a highly evolved peraluminous pluton: the Belvís de Monroy leucogranite (Cáceres, Spain). Lithos 179, 137–156. http://dx.doi.org/10.1016/j.lithos.2013.08.004.

Merino, E., Villaseca, C., Orejana, D., Pérez-Soba, C., Belousova, E., Andersen, T., 2014. Tracing magma sources of three different S-type peraluminous granitoid series by in situ U–Pb geochronology and Hf-isotope zircon composition: the Variscan Montes de Toledo Batholith (central Spain). Lithos (accepted for publication).

Orejana, D., Merino, E., Villaseca, C., Pérez-Soba, C., Cuesta, A., 2011. Electron microprobe monazite geochronology of granitic intrusions from the Montes de Toledo Batholith (central Spain). Geol. J. 47, 41–58. http://dx.doi.org/10.1002/gj.1331.

Perconig, E., Vázquez, F., Velando, F., Leyva, F., 1983. Sobre el descubrimiento de fosfatos sedimentarios en el Precámbrico Superior de España. Bol. Geol. Min. 114, 187–207.

Perconig, E., Vázquez, F., Velando, F., Leyva, F., 1986. Proterozoic and Cambrian phosphorites-deposits: Fontanarejo, Spain. In: Cook, P.J., Shergold, J.H. (Eds.), Phosphate Deposits of the World 1. Cambridge University Press, Cambridge, pp. 220–234.

Rambaud, F., Caraballo, J.M., Barrera, J.L., 1983. Los yacimientos de cuarzo-apatito (fosforita) en el Macizo Hespérico Español: el caso de Aldea Moret-Zarza la Mayor (Cáceres). Cuad. Lab. Xeolóxico Laxe 6, 387–408.

Ramírez, J., Menéndez, L.G., 1999. A geochemical study of two peraluminous granites from south-central Iberia; the Nisa-Albuquerque and Jalama batholiths. Mineral. Mag. 63, 85–104.

Rodriguez, L.R., López, F., Martín, J., Rubio, F., 2008. Mapa Geológico de la Península Ibérica, Baleares y Canarias, E: 1: 1.000.000. Inst. Geol. Min. España, Madrid.

Rodríguez-Alonso, M.D., Díez Balda, M.A., Perejón, A., Pieren, A., Liñán, E., López Díaz, F., Moreno, F., Gámez, J.A., González Lodeiro, F., Martínez Poyatos, D., Vegas, R., 2004. La secuencia litoestratigráfica del Neoproterozoico-Cámbrico Inferior. In: Vera, J.A.(Ed.), Geología de España. SGE-IGME, Madrid, pp. 78–81.

Rønsbo, J.G., 2008. Apatite in the Ilímaussaq alkaline complex: occurrence, zonation and compositional variation. Lithos 106, 71–82. http://dx.doi.org/10.1016/j.lithos.2008.06.006.

Sha, L.-K., Chappell, B.W., 1999. Apatite chemical composition, determined by electron microprobe and laser-ablation inductively coupled plasma mass spectrometry, as a probe into granite petrogenesis. Geochim. Cosmochim. Acta 63, 3861–3881. http://dx.doi.org/10.1016/S0016-7037(99)00210-0.

Sharp, Z.D., 1990. A laser-based microanalytical method for the in situ determination of oxygen isotope ratios of silicates and oxides. Geochim. Cosmochim. Acta 54, 1353–1357. http://dx.doi.org/10.1016/0016-7037(90)90160-M.

Sharp, Z.D., Essene, E.J., Kelly, W.C., 1985. A re-examination of the arsenopyrite geothermometer: pressure considerations and applications to natural assemblages. Can. Mineral. 23, 517–534.

Shepherd, T., 1981. Temperature programable heating-freezing stage for microthermometric analysis of fluid inclusions. Econ. Geol. 76, 1244–1247. http://dx.doi.org/10.2113/gsecongeo.76.5.1244.

Tornos, F., Delgado, A., Casquet, C., Galindo, C., 2000. 300 million years of episodic hydrothermal activity: stable isotope evidence from hydrothermal rocks of the Eastern Iberian Central System. Miner. Deposita 35, 551–569. http://dx.doi.org/10.1007/s001260050261.

Trotter, J.A., Eggins, S.A., 2006. Chemical systematics of conodont apatite determined by laser ablation ICPMS. Chem. Geol. 233, 196–216. http://dx.doi.org/10.1016/j.chemgeo.2006.03.004.

Ubide, T., 2013. The Cretaceous Alkaline Magmatism in Northeast Iberia. Igneous Processes and Geodynamic Implications. Doctoral Thesis Universidad de Zaragoza, Zaragoza.

Ugidos, J.M., Valladares, M.I., Recio, C., Rogers, G., Fallick, A.E., Stephens, W.E., 1997. Provenance of Upper Precambrian–Lower Cambrian shales in the Central Iberian Zone, Spain: evidence from a chemical and isotopic study. Chem. Geol. 136, 55–70. http://dx.doi.org/10.1016/S0009-2541(96)00138-6.

Van Achterbergh, E., Ryan, C.G., Griffin, W.L., 2001. GLITTER Version 4. Macquarie Research Ltd., Sidney.

Villaseca, C., 2011. On the origin of granite types in the Central Iberian Zone: contribution from integrated U–Pb and Hf isotope studies of zircon. Libro actas VIII Congreso Ibérico de Geoquímica 2011, 29–34.

Villaseca, C., López-García, J.A., Barbero, L., 2005. Estudio de la composición isotópica (Pb-S-O) de las mineralizaciones de Pb-Zn de Mazarambroz (Banda Milonítica de Toledo). Geogaceta 38, 271–273.

Villaseca, C., Pérez-Soba, C., Merino, E., Orejana, D., López-García, J.A., Billstrom, K., 2008. Constrasting crustal sources for peraluminous granites of the segmented Montes de Toledo Batholith (Iberian Variscan Belt). J. Geosci. 53, 263–280. http://dx.doi.org/10.3190/jgeosci.035.

Villaseca, C., Merino, E., Oyarzun, R., Orejana, D., Pérez-Soba, C., Chicharro, E., 2014. Contrasting chemical and isotopic signatures from Neoproterozoic metasedimentary rocks in the Central Iberian Zone (Spain) of pre-Variscan Europe: implications for terrane analysis and Early Ordovician magmatic belts. Precambrian Res. 245, 131–145. http://dx.doi.org/10.1016/j.precamres.2014.02.006.